Exacerbation of levee failure with climate change: Insights from ERT monitoring

Authors: Adrian White*[a, b], Paul Wilkinson[a], James Wookey[b], John Michael Kendall[c], Ross Stirling[d], James Boyd[a], Joel Smethurst[e], Jonathan Chambers[a]

a. British Geological Survey, Nottingham, United Kingdom
b. University of Bristol, Bristol, United Kingdom
c. University of Oxford, Oxford, United Kingdom
d. Newcastle University, Newcastle, United Kingdom
e. University of Southampton, Southampton, United Kingdom

* Corresponding author

This is a non-peer-reviewed preprint submitted to EarthArXiv. The manuscript has been submitted to the Journal of Engineering Geology.

Abstract

Climate change is bringing hotter, drier summers and warmer, wetter winters, intensifying winter floods and causing larger seasonal variations in soil moisture. These shifts place increasing stress on levees – many of which were constructed decades or centuries ago – making their current performance challenging to assess. Levee performance depends on limiting water ingress, as increased seepage can trigger piping and slope failure, potentially leading to catastrophic breaches. Hydraulic conductivity strongly controls water ingress, but is challenging to measure directly and can change as the materials deteriorate. To investigate how environmental loading affects levee performance, a clay levee in northern England was monitored for four years every 48 hours using electrical resistivity tomography (ERT) – a geophysical technique sensitive to fluid changes – alongside environmental sensors (soil moisture, river stage, and meteorological data). Two zones showed clear responses to climatic and hydrological forcing: the foundation strata, where groundwater levels rose with river levels, and the active layer (upper ~1.5 m), which seasonally dried in summer and rewetted in winter. These zones may therefore be particularly vulnerable to future climatic extremes and flood events. Analysis of annual drying-front depths indicates that average summer desiccation depths could increase from ~0.6 m to >1 m in northern England by the late 21st century (UKCP18 data, RCP8.5). This enhanced desiccation may reduce their performance, especially in early autumn when open shrinkage cracks can act as seepage pathways during subsequent floods. Forward planning using geophysical methods will help guide remediation and mitigate the effects of potential failure in levees.

Keywords: Levee; flood embankment; climate change; ERT; drought; glacial till; soil moisture deficit.

1 Introduction

Levees (also known as flood embankments or dykes) are critical earthworks built to protect land, property, and infrastructure from floods up to a designed height or recurrence interval. However, when levees fail, particularly due to breaches, the resulting floods can cause significant damage, disrupt essential infrastructure, and lead to loss of life (Hui et al., 2016; Orlandini et al., 2015; Pistrika and Jonkman, 2010). Over time, levees deteriorate due to the prevailing environmental conditions such as the local climate, river and groundwater levels, wave height and burrowing animals (Bayoumi and Meguid, 2011; Simm et al., 2012) (Figure 1). The effects of this environmental loading are influenced by the levee's material properties, which control its ability to resist water ingress and maintain structural integrity during flood events.

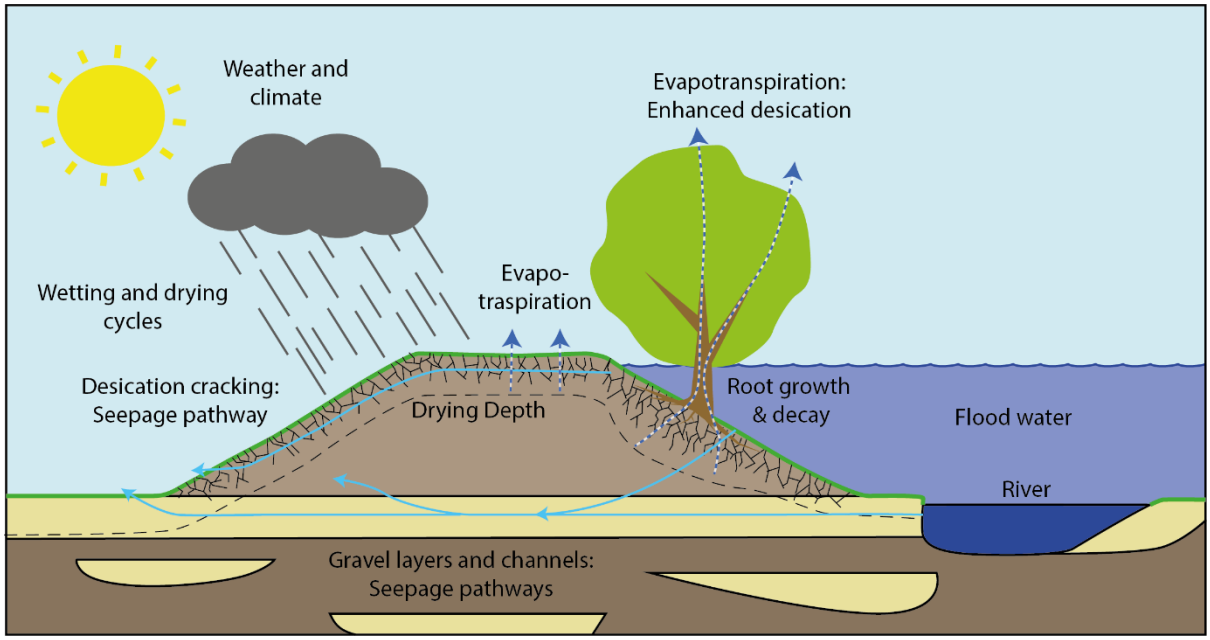

Figure 1. Schematic diagram showing the effects of environmental loading on a levee, which can drive deterioration processes. These processes can lead to greater hydraulic conductivity, which may facilitate water ingress during flood events. Climate change is altering weather and climate patterns, which may exacerbate these processes. © University of Bristol & British Geological Survey © UKRI

Levee materials can have a significant impact on levee performance. For example, poorly compacted, compressible, or organic soils can experience long-term settlement, increasing the risk of localised overtopping (Tarrant et al., 2017). Granular soils are more susceptible to seepage and internal erosion (suffusion), which increases hydraulic conductivity and may lead to piping failure (CIRIA et al., 2013; Johnston et al., 2021). Meanwhile, soils susceptible to shrink-swell can develop regions of elevated hydraulic conductivity in the near surface layer through repeated moisture cycling (Dixon et al., 2019; Stirling et al., 2021), opening cracks (Yu et al., 2021) and degrading the soil structure (Dyer et al., 2009; Morris et al., 2007). High hydraulic conductivities are a major factor in non-overtopping levee failures during flood events (Bettess and Reeve, 1995; Zhang et al., 2016).

In addition to the direct impact of more frequent, larger floods (IPCC, 2023), climate change is also altering the environmental loading that levees are exposed to, which is particularly affecting soil moisture dynamics (Islam et al., 2024; Janga et al., 2024; Raković et al., 2024; Samaniego et

al., 2018). The UK, for example, will face hotter, drier summers and warmer, wetter winters, exacerbating seasonal moisture cycles (Lowe et al., 2018). These shifts, especially prolonged droughts, will lead to more pronounced wetting and drying cycles in levee soils, promoting desiccation crack formation and increasing hydraulic conductivity (Stirling et al., 2021). Over time, these processes have the potential to accelerate levee deterioration and heighten the risk of failure (Robinson and Vahedifard, 2016; Rouainia et al., 2020).

Understanding the subsurface moisture dynamics of levees is critical for predicting areas at risk of long-term deterioration due to seasonal cycles enhanced by climate change (Lowe et al., 2018). Electrical Resistivity Tomography (ERT) can be used to monitor the internal moisture dynamics of levees and embankments (Amabile et al., 2020; Gunn et al., 2015; Tresoldi et al., 2019). ERT images bulk resistivity values of the soil, which is sensitive to lithology, porosity, pore fluid conductivity, moisture content and temperature (Waxman and Smits, 1968). By comparing repeat measurements, applying a correction for the effects of temperature variation, and assuming constant pore fluid conductivity, the resistivity changes can be interpreted as moisture content changes, providing insight into the levee's internal moisture dynamics (Chambers et al., 2014; Jodry et al., 2019).

In this paper, we present the findings from a 4-year monitoring study of a clay levee in northern England. Combining ERT monitoring with environmental sensor data, we assess the levee's moisture dynamics and explore whether potential failure mechanisms are active. These results have broad applicability to levees worldwide. We also consider the implications of climate change on long-term levee performance and explore strategies to mitigate them.

2 Field site

The levee selected for this study is located on the River South Tyne at Warden, 3 km northwest of Hexham, UK (Figure 2). The river reach at Warden is a local narrowing in the floodplain, increasing the flood risk (Figure 2B). The 600 m long ~2.5 m high levee protects 33 houses and the train line from Newcastle to Carlisle from flooding (Environment Agency, 2016).

This levee was selected due to its long history of flood events (Table 1), its recent (2007) reconstruction to modern standards and its material composition, which is a low to intermediate plasticity clay likely sourced from local glacial till. Glacial till is widespread across much of the UK, so this levee is likely representative of a significant proportion of UK levees, with the caveat that many levees have unknown compositions.

The first levee at Warden was built around 1950 from silt and sands following a snowmelt flood in 1947 (Archer et al., 2007a) (Table 1). In 2005, the embankment breached, and although the failure mechanism is unknown (Table 1, Figure 2C) over-steepened slopes (p.c. landowner), rabbit burrows (Mott Macdonald, 2019), and overtopping (Archer et al., 2007a) followed by external erosion have all been suggested. The current levee was re-constructed in 2007 using 18,000 tonnes of imported 'clay' (Evening Chronicle, 2007), and was designed to protect against 1 in 100 year floods (Environment Agency, 2020).

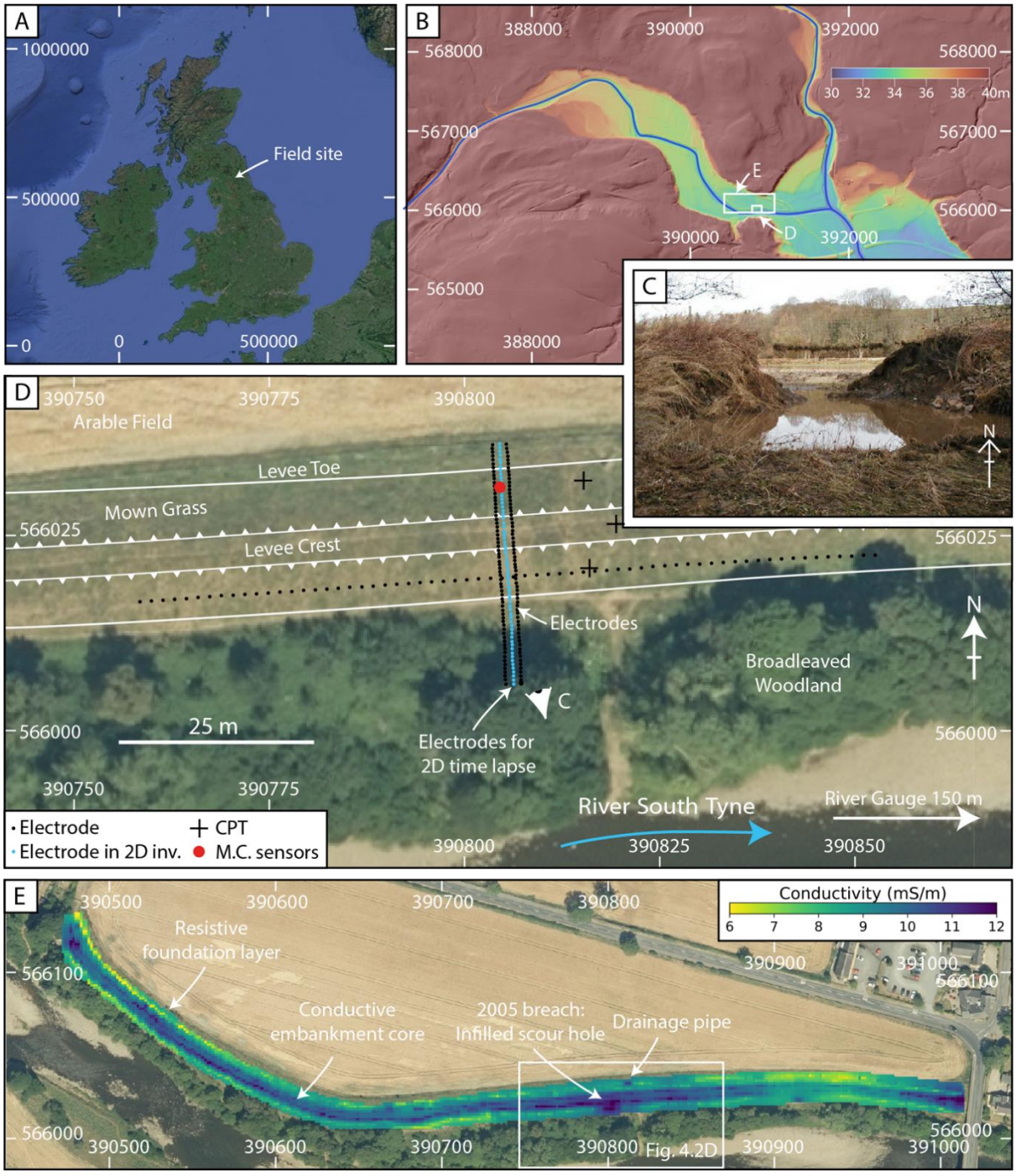

Figure 2. Overview of the field site at Warden, Northumberland. A) Location of the field site in the UK. B) Digital Terrain Model (DTM) of the river valley, showing the levee located at a narrowing within the valley. C) Photograph of the 2005 breach looking North (Part D for location) from the riverside through the embankment; image from the International Levee Performance Database (Özer et al., 2019). D) Map of the monitoring section, showing installed instrumentation. CPT = Cone Penetration Test, M.C. = Moisture content, and electrodes are for ERT monitoring. E) Electromagnetic (EM) conductivity survey results, for a depth of investigation of 1.2 m (White et al. 2023). Copyright attribution: Part A) satellite imagery Google Maps © 2022 Data SIO, NOAA, U.S. Navy, NGA, GEBCO, Landsat / Copernicus, Imagery©2022 Terra Metrics, Map data ©2022 Google, GeoBasis-DE/BKG. Coordinate system: British National Grid. Part B) Lidar base map © Environment Agency copyright and/or database right 2022. All rights reserved. UKRI. Part D & E) Aerial photography © UKP/Getmapping Licence No. UKP2006/01. Figure © University of Bristol & British Geological Survey ©

Date	Event	Details
1947	Flood	Snowmelt
c. 1950	Embankment constructed	First levee constructed at the site
1955	Flood	Peak River level 5.61 m - 8 properties flooded, mechanism unknown
8 January 2005	Flood	Peak River level 5.52 m Embankment breached (Figure 1D) - 23 properties flooded
2007	Embankment replaced	Levee replaced and raised
23 June 2012	Flood	Peak River level 4.20 m - Water at embankment toe
18 May 2013	Flood	Peak River level 4.65 m - Water against embankment
05 December 2015	Flood	Peak River level 5.71 m - Water against embankment, flood walls adjacent to the embankment overtopped, 14 properties flooded

Table 1. Flood and embankment history of the River South Tyne at Warden. River stage base level 34.8 m above Ordinance Datum (AOD) (Archer et al., 2007b, 2007a; Environment Agency, 2016; Northumberland County Council, 2016).

The levee has been characterised along its length using geotechnical methods, including cone penetration testing and trial pits, and geophysical methods, including electro-magnetic imaging (EMI), ERT and multi-channel analysis of surface waves (White et al., 2023). These surveys, illustrated by the EMI (Figure 2E), show that the embankment properties are similar along its entire length. The EMI also shows a conductive anomaly, ~15 m wide, interpreted as the infilled scour hole produced during the 2005 breach.

Overall, the embankment comprises a relatively homogenous compacted core covered by a plastic geogrid to prevent animal burrowing and topped with ~30 cm of topsoil. The core is glacial till (10% gravel, 34% sand, 30% silt, 26% clay, and the occasional cobble) with a liquid limit of 35%, a plastic limit of 20%, and a plasticity index of 15, making it a low to intermediate plasticity clay. The levee is grass-covered and mown a few times a year to maintain erosion protection (Simm et al., 2017; Smith et al., 2009); between the river and the levee are trees and shrubs. The levee foundations are superficial alluvial and river terrace deposits (Burns and Miller, 1883), comprising sands and gravels. Detailed mapping upstream of the site found seven different river terrace levels, the oldest thought to have formed during late Pliocene deglaciation (Passmore and Macklin, 2000). The riverbank shows a stratigraphy of silts, sands and gravels with large cobbles and boulders, typical of river channel and floodplain deposits. The bedrock geology is the Stainmore Formation, comprising limestones, mudstones and sandstone (British Geological Survey, 1975), and is likely too deep to affect the embankment performance.

3 Methodology

The characterisation survey identified a ~100 m section of the levee where it crosses a palaeochannel, is at its tallest point, and is also the location of the 2005 breach (Figure 2D). All these factors can increase the risk of a breach developing, so this section was selected for monitoring. It was instrumented in the autumn of 2021 with an ERT monitoring system and geotechnical sensors (Figure 2D) (Blake et al., 2022). Full data collection started in November 2021.

3.1 Environmental sensors

This site was instrumented with an array of environmental sensors (Blake et al., 2022), including two volumetric moisture content (VMC) sensors installed in the landward slope 0.1 m and 0.3 m below the surface, along with a 1D temperature array comprising six sensors extending to 4 m below the surface (Figure 2D, Figure 5B). A pre-existing river gauge was located 150 m downstream of the site on the river bridge maintained by the UK Environment Agency (River Levels, 2024). Weather data are extracted from the 1 km HadUK database, which provides daily temperature and rainfall data for the UK (Met Office et al., 2018). The HadUK data was chosen over a local weather station as it is a daily data set spanning over six decades, allowing for integration with the UKCP18 climate data (Met Office et al., 2018).

3.2 Evapotranspiration and Soil Moisture Deficit

To assess the hydrological forcing on the levee, both the addition of moisture to the surface through rainfall (measured) and the removal of moisture through evapotranspiration (calculated) need to be known (Holmes et al., 2022). Evapotranspiration is the combination of evaporation from the soil surface and transpiration from vegetation (Allen et al., 1998). Evapotranspiration is controlled by weather conditions (e.g. solar radiation, air temperature, humidity, and wind speed), and vegetation type and state. The Penman-Monteith equation is used to calculate the reference evapotranspiration (Allen et al., 1998), using data from the 1 km HadUK Grid, including daily minimum and maximum temperatures (Met Office et al., 2018). The other environmental parameters that can affect evapotranspiration are unavailable in this long-term dataset, so the default parameters described in Allen et al., (1998) are used. The reference evapotranspiration is multiplied by a crop coefficient to estimate actual evapotranspiration. The crop coefficient is assumed to be constant with a value of one, year-round; this is a commonly used simplification for grass-covered geotechnical assets (Helm et al., 2016; Smethurst et al., 2006).

The soil moisture deficit (SMD) is derived using a simple bucket model to calculate the cumulative effect of rainfall and evapotranspiration (Allen et al., 1998; Clarke and Smethurst, 2010). This model assumes that on the first day of monitoring in early November, SMD = 0, each day, rainfall (P) is added, and evapotranspiration (ET) is subtracted. If SMD > 0, we assume the excess rain leaves the site as runoff, and SMD returns to zero. However, if SMD < 0, the moisture deficit carries over to the following day. During dry periods, the SMD will become increasingly negative, but there is finite water within the rooting depth (assumed to be 1 m). For a typical silty clay, the total available water (TAW) within the rooting zone is 0.16 m^3/m^2 (160 mm) (Allen et al., 1998). When the SMD reaches 160 mm, the grass wilts, and evapotranspiration stops. Before SMD reaches 160 mm, the grass will become increasingly water stressed and the evapotranspiration rate will slow. Water stress occurs when the SMD exceeds the readily available water (RAW). For pasture, RAW can be assumed to be 0.6×TAW (Allen et al., 1998). To reflect the effect of water stress on the SMD when TAW > SMD > RAW, a modified crop factor (K_s) is used,

$$K_s = \frac{TAW - SMD}{TAW - RAW}, \quad (1)$$

to reduce the rate of evapotranspiration (Allen et al., 1998). This SMD bucket model assumes no groundwater recharge (Clarke and Smethurst, 2010), although this may occur, especially during the wetter months.

3.3 Resistivity monitoring

An ERT monitoring system, PRIME (Proactive Infra-structure Monitoring and Evaluation), was installed along the levee. Here, the monitoring array comprised four lines, three perpendicular to the levee and one parallel (Figure 2D). Each line contained 64 electrodes with a spacing of 0.5 m (perpendicular lines) or 1.5 m (parallel line). For each line, a dipole-dipole survey was used with dipole lengths of a = 1–3 electrode spacings and inter-dipole spacings na, where n = 1–7 (Loke et al., 2013). The dipole-dipole measurement configuration was chosen for its good image resolution and efficient use on a multichannel instrument, reducing overall power consumption (Dahlin and Zhou, 2004). Over the monitoring period, ERT measurements were collected every 48 hours, resulting in 686 repeat measurement sets. Due to reduced power availability, the measurement frequency was changed to every 72 hours from January to March 2022. The data was sent to a remote server via a 4G mobile connection. During the monitoring period, water was never against the levee or covering the electrode array.

ERT data processing, filtering and inversion used ResIPy (Blanchy et al., 2020), an open-source software wrapper and GUI for R3t, and R2, which are 3D and 2D inversion codes, respectively (Binley and Slater, 2020; Blanchy et al., 2020). Measurements were removed prior to inversion if there was no reciprocal measurement or the reciprocal error exceeded 5% (Tso et al., 2017). A power law error model was fitted to the reciprocal errors at each time step; this was combined with a numerical modelling error estimate from the mesh using gaussian error propagation (Binley and Slater, 2020; Blanchy et al., 2020). The 2D timelapse used a difference inversion, where the difference between the current time step and a baseline was inverted (LaBrecque and Yang, 2000). The baseline was set to 20 April 2022 and was used to calculate resistivity change unless stated otherwise. Overall, each time step converged with a mean χ^2 of 1.07 and a standard deviation of 0.16.

3.3.1 Temperature modelling

Resistivity measurements are sensitive to changes in temperature. For soils at temperatures between 0-50°C, conductivity increases by ~2% for every 1°C increase in temperature (Ma et al., 2011). To reduce temperature-induced resistivity changes a simplified 1D seasonal temperature model can be fitted to the temperature array data (Figure 3) (Brunet et al., 2010):

$$T(t,z) = T_{\text{mean}} + Ae^{-\left(\frac{z}{d}\right)}\sin\left(\frac{2\pi}{365.25}t + \varphi - \frac{z}{d}\right), \quad (2)$$

where $T(z,t)$ is the temperature at day t and depth z, T_{mean} is the mean annual temperature, A is the amplitude of the sinusoidal variation in yearly air temperature, d is the characteristic penetration depth of the temperature variations, φ is the phase offset and $(\varphi - z/d)$ is the phase lag. The resulting fitted parameters are listed in Table 2. This approach is now routinely used for temperature corrections (Chambers et al., 2014; Jodry et al., 2019; Uhlemann et al., 2017).

Parameter	T_{mean} (°C)	A (°C)	d (m)	φ (rad)
Value	9.95	6.42	3.13	-1.94

Table 2 Fitted parameters for the temperature model

However, in 2025, the spring and summer months were unusually warm. This caused a significant departure from the model (Figure 3) to depths of at least 2.5 m. To account for this, we adopted an alternative approach, solving the 1D heat equation numerically using a Backward Time Centred Space (BTCS) finite difference scheme (BTCS is a stable implicit Euler method). The 1D model was split into seven depth domains, the first from the surface to the first temperature sensor, the second from the first to the second temperature sensor, and so on until the last domain which spanned from the sixth temperature sensor to a base depth (16 m) where the temperature was assumed to be constant.

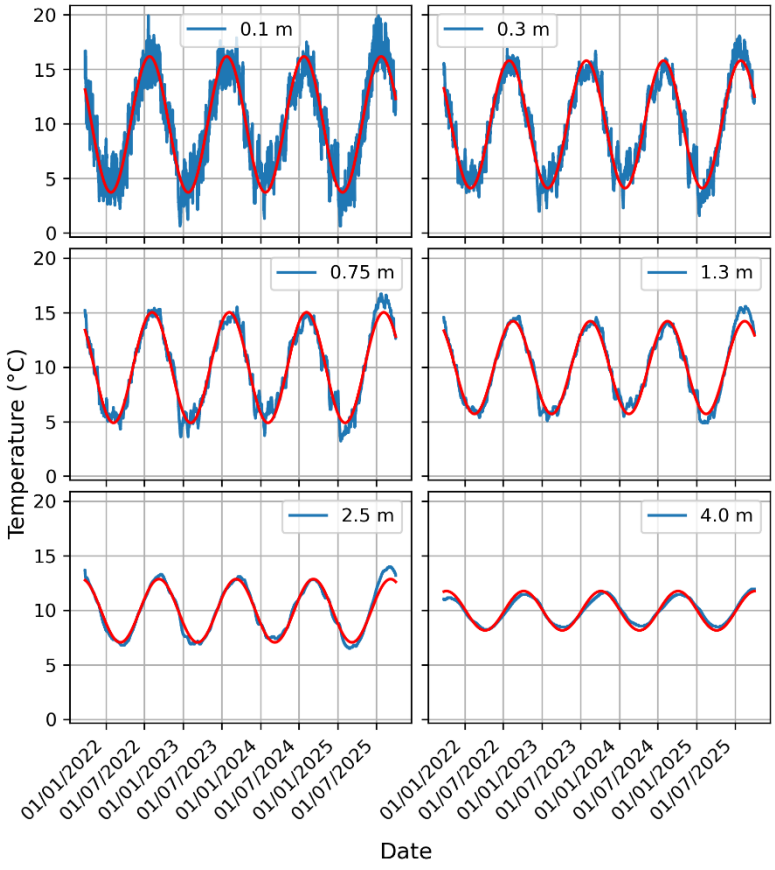

Figure 3. Temperature data from the six sensors installed at different depths (blue) and the fitted 1D temperature model (red). © University of Bristol & British Geological Survey © UKRI

Each depth domain was discretised into 50 segments. The Dirichlet boundary conditions for each domain were set to the air temperature at the surface, the measured temperatures at the depths of each temperature sensor, and T_{mean} at the base depth. The thermal diffusivity was calculated from d, the characteristic depth fitted in the seasonal model (Equation 2) as $\alpha = \pi d^2/365.25$, and the initial temperature distribution was calculated from the seasonal model applied at the first time-step (2021/09/24 00:00). A time interval of 0.1 days was used to capture diurnal as well as longer period variations. The differences between the BTCS model and the seasonal model and are illustrated in Figure 4.

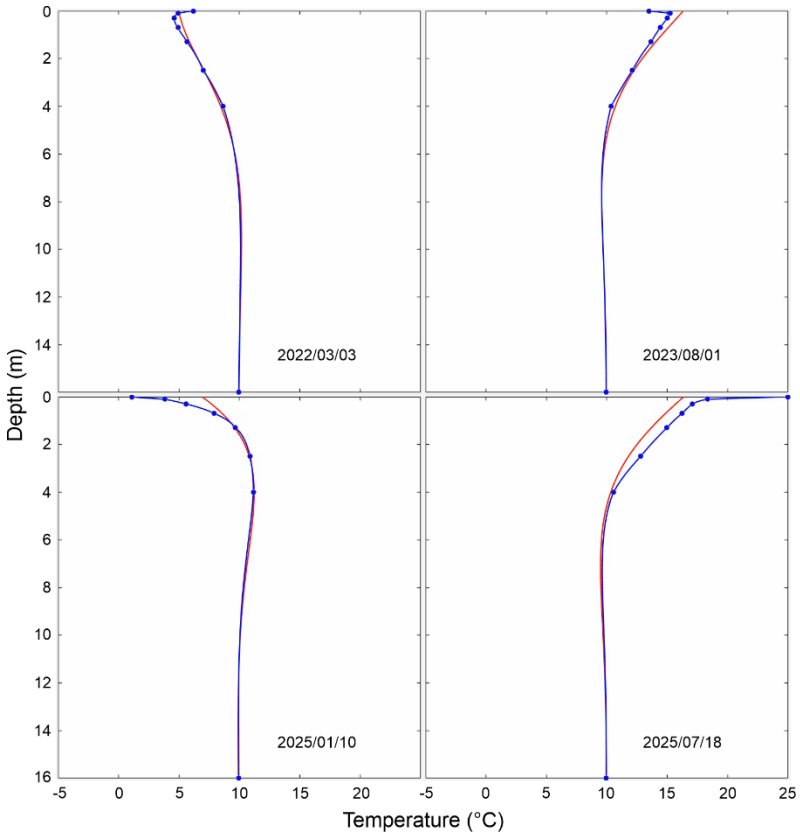

Figure 4. BTCS (blue line) and seasonal (red line) temperature models. Blue dots indicate air temperature (depth = 0 m), measured ground temperatures (0.1 - 4 m), and T_{mean} (16 m). Note the greater departures from the seasonal model in 2025. © University of Bristol & British Geological Survey © UKRI

The temperatures for the centroid depth of every cell at each time step were interpolated from the BTCS temperature model results. The resistivity value of each cell was then adjusted to the mean annual temperature of 9.95°C, resulting in a maximum resistivity change of ~20%.

4 Results

4.1 Levee structure

To assess the structure of the levee, the baseline survey was inverted as a single 3D resistivity model (Figure 5A). This confirms that the levee is relatively homogenous with a ~20 Ωm embankment sitting on top of higher resistivity material. Where the perpendicular and parallel lines cross, there is a higher resistivity region, however, ERT inversions are affected by data distribution, offline topography, and isotropic smoothing, so we need to consider the reliability of this 3D model (Bièvre et al., 2018; Hojat et al., 2020).

Comparing a cross-section along the central perpendicular line of electrodes (high data density) to a location away from the perpendicular electrodes (low data density) demonstrates a large difference in resistivity structure (Figure 5A). The cross-section along the central perpendicular line of electrodes has higher resistivity values (~200 Ωm) in the foundation layer and closely matches a 2D model containing only the data of the same central perpendicular line, and the structure is consistent with the CPT-derived logs (Figure 4B). In contrast, the cross-section away

from the perpendicular line of electrodes shows that the 3D model has a cylindrical resistivity distribution centred on the levee parallel line, and quickly converges to 100 Ωm, the starting resistivity value of the ERT model. This cylindrical resistivity distribution is a direct result of the levee parallel line being straight with no azimuthal sensitivity (i.e., it cannot discriminate between anomalies to either side or below) and an isotropic L2 smoothing regularisation. Therefore, the range of resistivity values from the foundation material will likely be underestimated away from the perpendicular ERT lines (White et al., 2024) (Figure 5A).

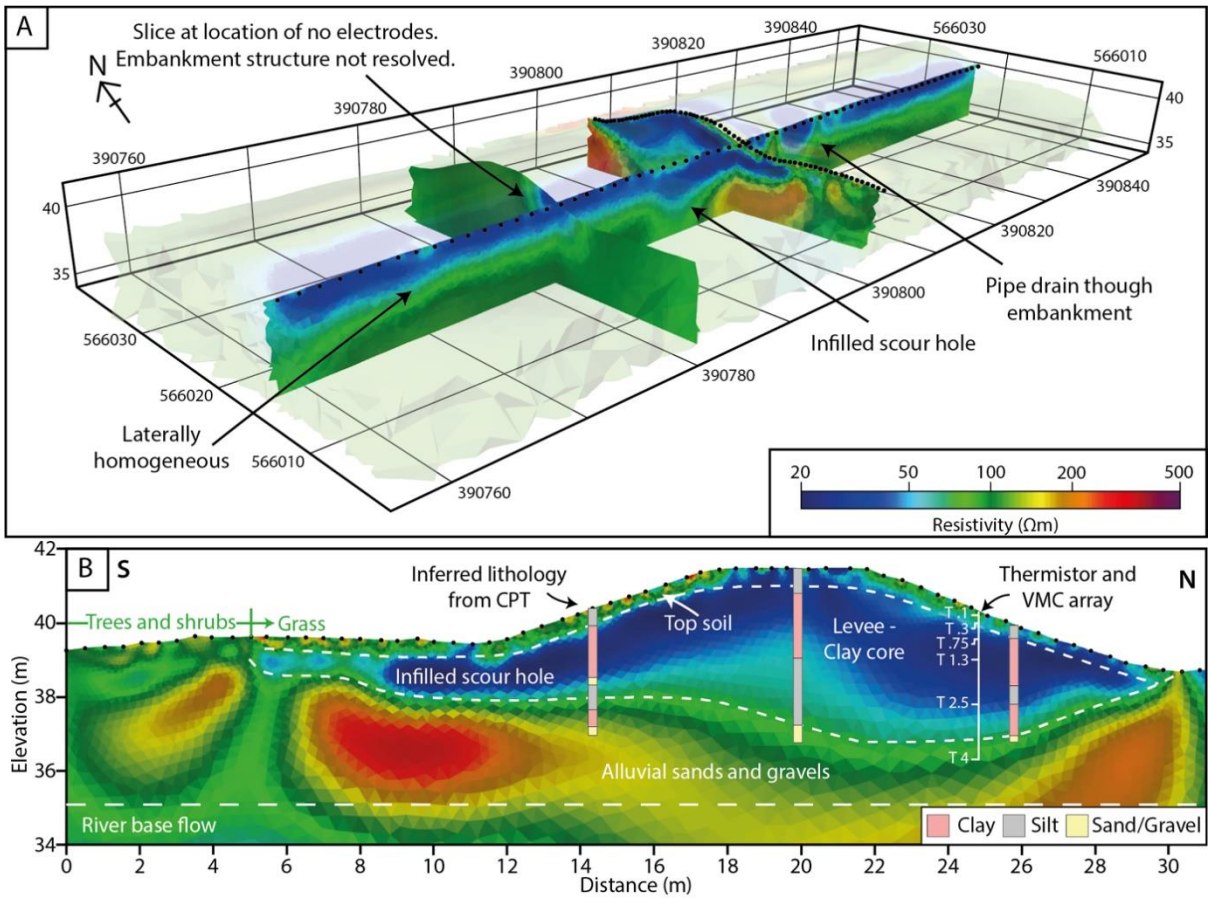

Figure 5. ERT inversions of the baseline timestep (20th April 2022). A) 3D model of the levee. To aid visualisation, the 3D model has been sliced along the levee parallel line, the central perpendicular line, and a location away from the perpendicular lines. B) 2D model containing data from the central perpendicular line. The 2D inversion is overlain with CPT-derived logs with interpretation and the river level at a typical baseflow level. © University of Bristol & British Geological Survey © UKRI

The 3D model confirms that the levee is relatively homogeneous along the monitored section (when considering the effects of the array geometry) with small perturbations caused by the infilled scour hole and the drainage pipe under the levee (Figure 5A). Therefore, due to the computational efficiency of the 2D inversion for time-lapse monitoring and its good agreement with the 3D model, we present the 2D inversion results from the central perpendicular line.

~~Interpreting~~ The baseline 2D resistivity model with the CPT-derived logs – where the soil behaviour type was calculated and simplified using the approach of Robertson (1990) – suggests that the levee has three principal units (Figure 5B): 1) a low resistivity unit of 20-50 Ωm representing the clay fill of the levee; 2) a surface layer with intermediate resistivity values (~100 Ωm) representing the layer of topsoil covering the levee; and 3) a high resistivity layer

below the levee with values between 100-500 Ωm, highlighting the alluvial sand and gravel deposits. The low resistivity levee body cuts into the foundation layer, likely the result of topsoil removal during construction, following best practice guidance (CIRIA et al., 2013, fig. 10.26), and the infilling of the scour hole that formed during the original break.

4.2 Levee monitoring

4.2.1 Environmental monitoring

The hydrological and weather data show seasonal variations in rainfall, river level and soil moisture content over the monitoring period (Figure 6). In the summer months, rainfall is lower and evapotranspiration is higher, resulting in drying of the levee surface. In the autumn, the evapotranspiration decreases and rainfall increases, wetting up the surface of the levee and causing elevated water levels in the river that fluctuate throughout winter. During the monitoring period, there was no water against the levee; for flooding to be possible, the river level must exceed an elevation of 40 m above ordnance datum.

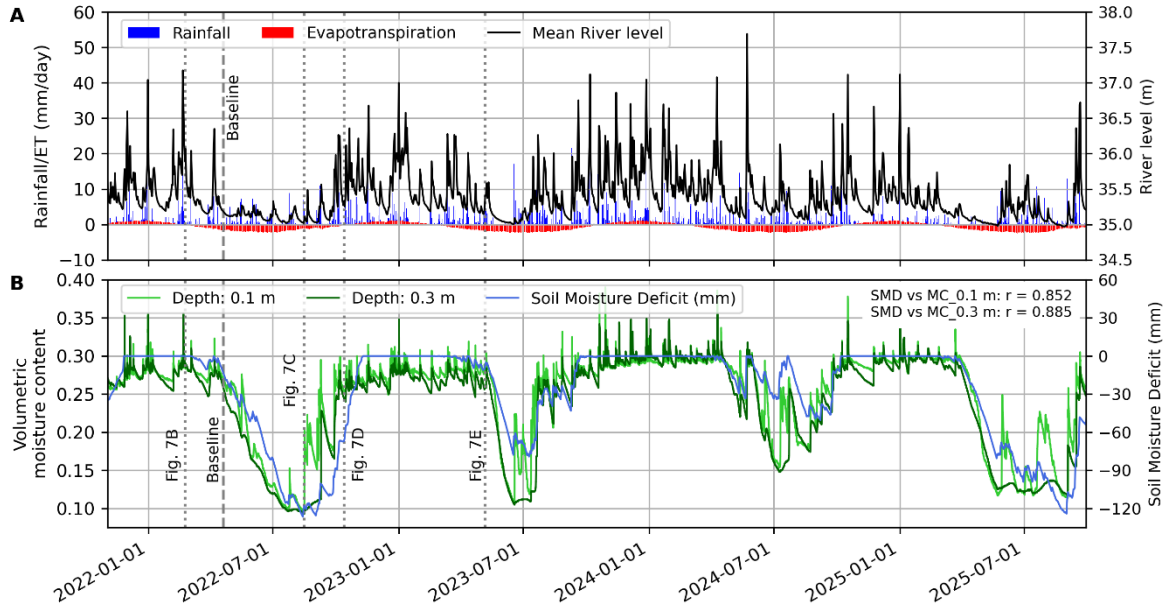

Figure 6. Environmental monitoring of the field site . A) Plots of rainfall, evapotranspiration and river level. B) Plots of the volumetric moisture content at 0.1 m and 0.3 m depths and the soil moisture deficit (SMD) derived using the Penman-Monteith equation. r = Pearsons correlation coefficient. Vertical dashed lines are the datasets shown in Figure 6. © University of Bristol & British Geological Survey © UKRI

Between autumn and spring, both moisture content sensors recorded average values of ~0.29 VMC (volumetric moisture content); this will approximate field saturation (Figure 6), which is typical of UK earthwork infrastructure (Smethurst et al., 2012). Heavy rainfall can cause values to spike above 0.3 VMC followed by a rapid drop. During summer, VMC drops gradually, correlating with decreased rainfall and increased evapotranspiration; this is the main drying cycle. During the summer, there are rapid fluctuations in surface moisture content caused by summer rainfall that is rapidly removed through high evapotranspiration rates. In the autumn, with the onset of more persistent rain, the surface appears to wet up rapidly, preceding the deeper VMC sensor.

4.2.2 Resistivity monitoring

Repeat ERT inversions reveal changes in resistivity values that correspond with changes in moisture content resulting from seasonal variations, weather events and changes in river level (Figure 7). The results from 20 April 2022 are used as the baseline to calculate the resistivity difference. This baseline was selected because the levee was still relatively saturated, representing winter conditions, and the river stage was close to its baseflow level (Figure 6). Baseflow is the typical streamflow between rainfall events. Surface drying from this baseline is associated with increasing resistivity values, while increases in river level or the water table result in decreasing resistivity values. The resistivity changes are not translated into absolute moisture content using a Waxman and Smits (1968) petrophysical relationship, which is commonly done (Chambers et al., 2014; Hojat et al., 2020; Holmes et al., 2022), due to the large variety of soil types and the corresponding modelling parameters (Boyd et al., 2024; Tso et al., 2019).

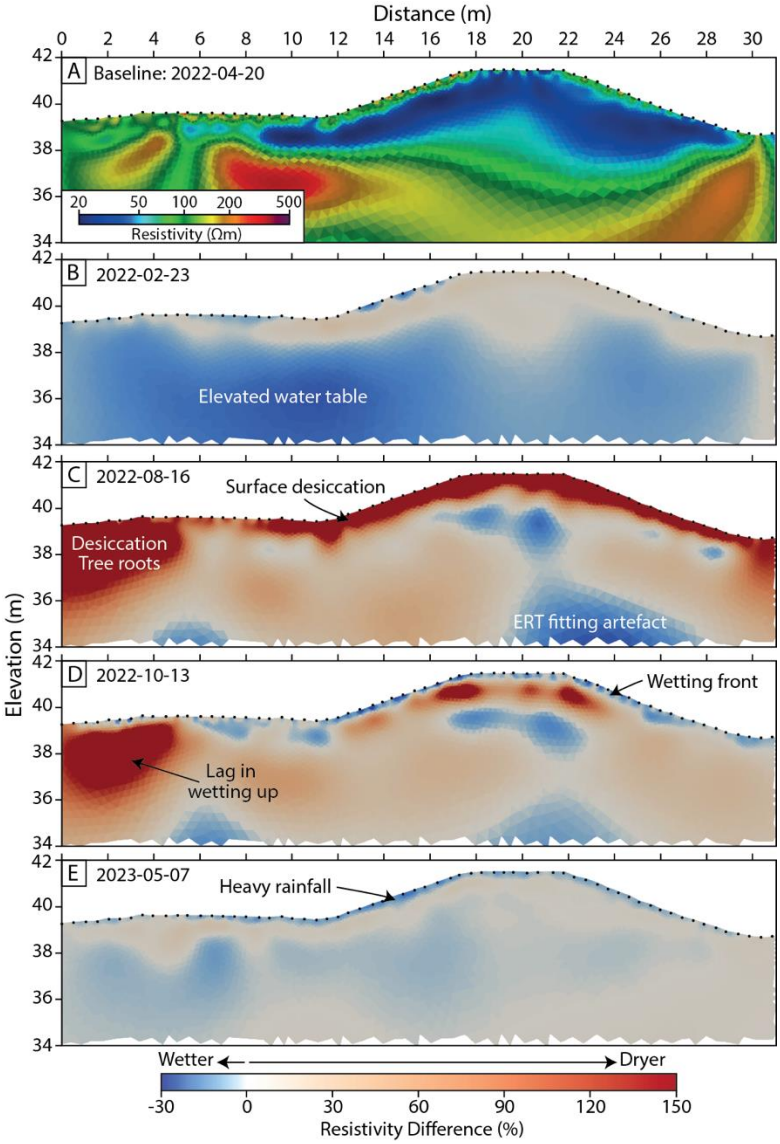

Figure 7. Selected timesteps from the timelapse inversion, with the temperature correction applied, illustrating the key processes imaged during the monitoring period. A) Baseline resistivity distribution, 20 April 2022. B) Winter flood event with an elevated water table (no water against the levee). C) End of summer dry period, with little rainfall.

D) Wetting up of the levee at the end of the summer. E) Effect of heavy rain on the near-surface. Figure 6 shows their alignment with the measured environmental parameters.

The ERT monitoring records the subsurface effects of seasonal cycles and short-term weather events. In the winter, the resistivity values in the foundation strata decrease and, after a particularly large rainfall event, decrease below the baseline values (Figure 7B). These decreases in resistivity span the width of the levee. During summer months, surface drying dominates, and at the end of the 2022 summer, after an extended period of dry weather, the surface shows large increases in resistivity values; these are deepest where there is woody vegetation (Figure 7C). At the end of the summer, with the reduction in evapotranspiration, a wetting front develops, wetting the levee from the surface downwards (Figure 7D). During heavy rainfall events, the near-surface records a transitory decrease in resistivity values associated with heavy rainfall (Figure 7E). ERT inversions are not free of artefacts; Figure 7C records a decrease in resistivity below the levee while the surface is very dry, this has been seen at other sites (Holmes et al., 2022), and is likely a result of slight overfitting of the data during the inversion.

5 Discussion

5.1 Levee variability: inferred failure mechanisms

To synthesise how the levee responds to changes in environmental conditions, the resistivity values from each cell in every time step can be combined by calculating the Coefficient of Variation (CV) (Boyd et al., 2021),

$$CV = 100\frac{\sigma}{\mu}, \quad (1)$$

where σ is the standard deviation, and μ is the mean value of each cell. The CV statistic allows a comparison of the relative variability of each cell despite large variations in different mean resistivity values (Figure 8). We would expect cells with large variabilities to be associated with relatively high hydraulic conductivities that facilitate moisture movement and/or to be exposed to larger hydrological forcings.

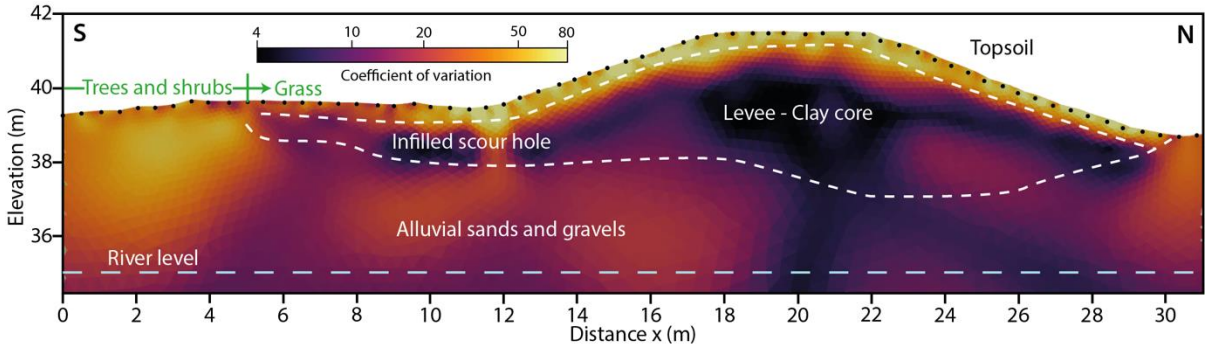

Figure 8. A plot of the coefficient of variation for each cell in the resistivity model shows areas of high and low variability. Labels and line work from Figure 5B.

The largest variabilities occur in the top ~1 m, which consists of a ~30 cm topsoil layer on top of the levee core. This region is directly exposed to fluctuations in surface conditions, so it will likely experience comparatively large hydrological forcings. Where there are trees and shrubs, this zone

extends over 3 m deep but is slightly less variable than in the grass covered embankment, which is consistent with the findings of Holmes et al. (2022). In contrast, the main levee body below 1 m shows very little variability, indicating that the compacted clay must have low hydraulic conductivity and is protected from environmental extremes by the overlying soil. The levee foundations show intermediate variability likely driven by changes in river level and associated groundwater conditions. This highlights two regions of the levee, the near-surface and the foundation strata, that respond to external environmental forcing and, therefore, facilitate moisture movement and may be at risk of long-term deterioration.

5.2 Foundation resistivity variation

To investigate the cause of the elevated temporal variability within the levee foundations (x = 12-30 m), changes in resistivity between time steps are compared to changes in river level. To summarise the resistivity data, the mean resistivity values for discrete elevation intervals are normalised by the corresponding baseline value and plotted on a time-elevation matrix plot Figure 9. Large peaks in the river level coincide with decreases in resistivity compared to the baseline values. Additionally, there are decreases in resistivity values between March and May 2023 and between September 2023 and April 2024, which correspond with above-average river levels (Figure 9), higher rainfall rates and elevated near-surface VMC (Figure 6). These periods of low resistivity values are likely caused by wetter than baseline soil conditions below ~39 m. Conversely, during the summer, there are small increases in resistivity throughout the foundation layer. Elevated river levels during these periods (e.g. October 2022) do not produce a large enough resistivity response to drop the measured resistivity values below the baseline values. These changes are separate from the direct surface drying, but suggest that significant air-filled porosity remains during short periods of elevated river levels.

Overall, despite the limitations of a 48-hour monitoring interval, the resistivity values appear to respond rapidly to elevated river levels. While the exact hydrological mechanism is not resolved, the strong correlation between river level and resistivity decrease and the known continuity of the resistivity decrease under the whole levee (Figure 5B) highlight foundation seepage as the most likely cause. Therefore, piping is a possible future failure mechanism for this levee. Fortunately, due to the upland location of this river, water levels rapidly recede, so water is only against the levee for short periods of time. This minimises the risk of seepage developing into a full piping failure due to insufficient time for internal erosion to occur (Semmens and Zhou, 2020). Inspection of the levee during and after flood events would be valuable for detecting any signs of piping failure. Additionally, rapid drawdown of the river level while moisture contents are maintained in the levee can induce shallow slope failures (Polemio and Lollino, 2011). Water has not been against the embankment during monitoring periods, so water retention within the levee slope cannot be investigated further.

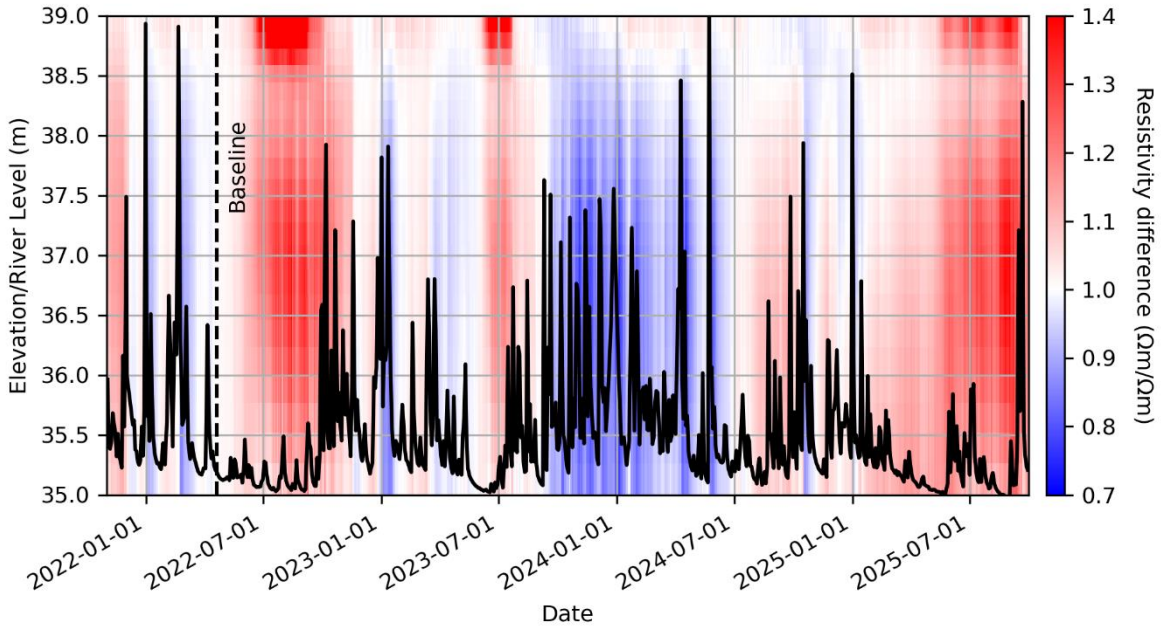

Figure 9. Elevation-date plot comparing changes in the average resistivity difference at discrete depth intervals within the foundation layer to changes in river level for each time step. Red = drier, blue = wetter. © University of Bristol & British Geological Survey © UKRI

5.3 Surface drying and cracking risk

To investigate the effect of surface drying on the levee, at each time step, the average resistivity values are calculated for discrete depth intervals in the top 1.5 m of the levee (x = 12-30 m), creating a 1D profile. Each of these profiles is normalised by the lowest mean resistivity value (i.e. approximately the highest moisture content) found at each depth interval over the monitoring period (

Figure 10A). The dominant moisture content cycle is characterised by a drying front that develops in spring through to the summer and a wetting front in autumn. Both fronts propagate from the surface downwards. The drying front is picked by a contour value of 1.5 Ωm/Ωm (Figure 10D). This value was selected as it is the minimum value that enables the surface drying processes to be separated from other background processes (e.g., uncorrected temperature anomalies, changes in pore-fluid chemistry, small saturation fluctuations), and from ~~the~~ floodplain aquifer processes below (Figure 10D).

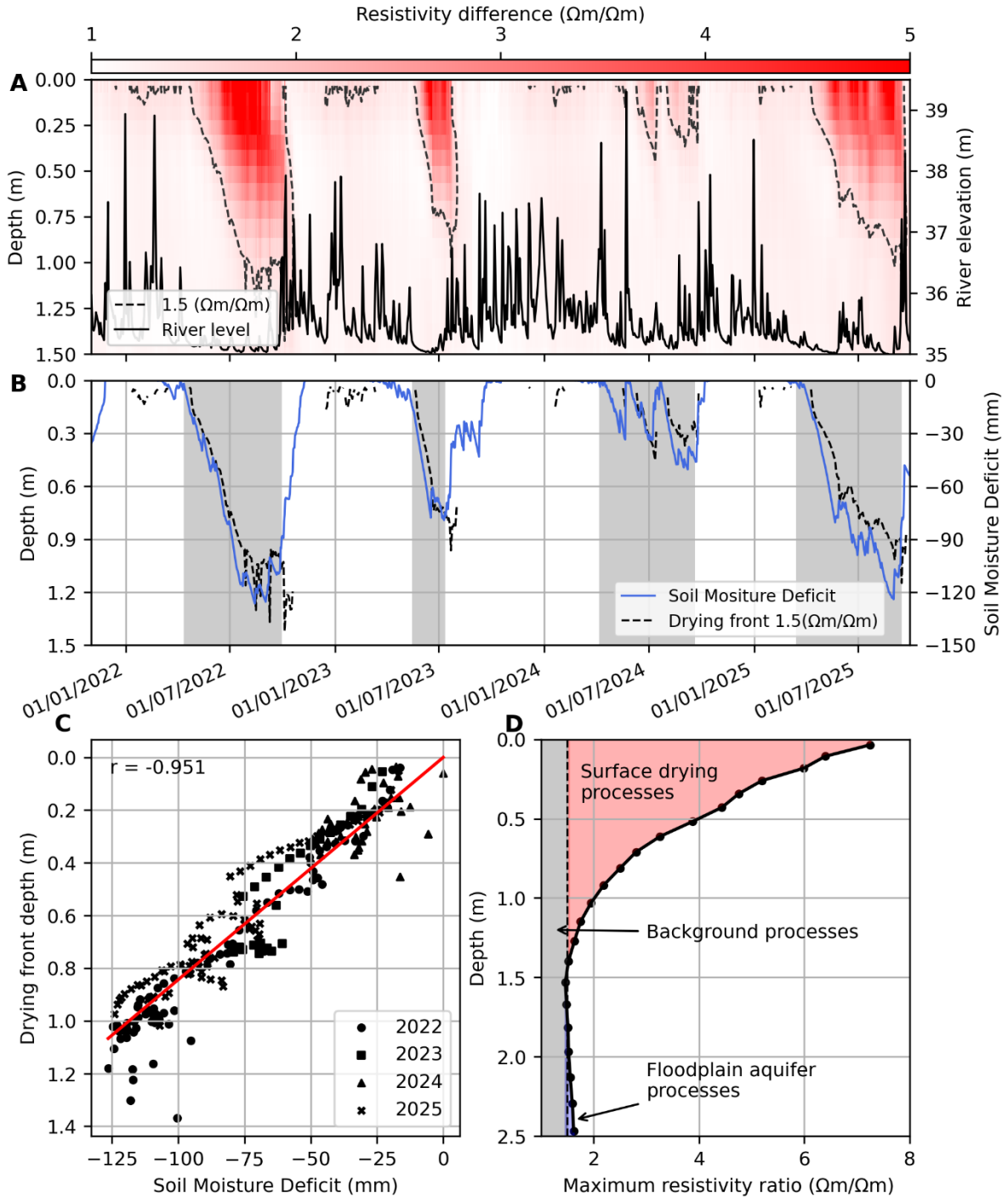

Figure 10. A) Depth versus time plot for the average resistivity difference at discrete intervals (normalised to the minimum resistivity in each row) for the top 1.5 m of the levee, data cropped between 12-30 m (Figure 7). The plot is overlain with the river level data. The black dashed line is the 1.5 Ωm/Ωm contour, representing drying depth. B) Comparison of the resistivity-derived drying depth (1.5 Ωm/Ωm) to the soil moisture deficit (SMD). The drying depth is filtered to remove the 1.5 Ωm/Ωm contour associated with wetting fronts. The shaded grey areas are used to correlate SMD with depth of drying front. C) Correlation plot between soil moisture deficit (SMD) and depth of drying front for each drying cycle that occurred within the three years. The days included are shaded grey in part B. The red line is a line of best fit, where r is the Pearsons correlation coefficient. D) Maximum resistivity difference at each depth of the model over the monitoring period. The top 1.5 m are shown in ~~Part~~ Panel A.

Desiccation of the upper soil layer does not compromise the performance of levees directly, but it is a necessary precursor for desiccation crack formation (Yu et al., 2021) that may facilitate seepage (Dyer et al., 2009) or affect vegetation cover that can reduce erosion resistance during overtopping events (Vannoppen et al., 2016). Direct measurement of cracks in the field is difficult; manual approaches have used thin push rods inserted into the cracks to estimate depth (Yu et al., 2021), while non-invasive tests have used high resolution ERT (Jones et al., 2014; Sentenac et al., 2012) and linear transducers to measure the crack opening (Stirling et al., 2018). Based on excavated desiccation cracks (Dyer et al., 2009), the full crack network could not be measured with current methods and will underestimate cracking depth. In contrast, imaging the drying depth provides a crack susceptibility depth in which desiccation cracks may form if the soil type and conditions are right (e.g. soil plasticity), providing a near maximum depth constraint.

Soil plasticity strongly correlates with the shrink swell properties of the soil (Thaimo et al., 2021), with cracking being particularly problematic in high plasticity clay soils (plasticity index >25) (Dyer, 2004). Cracking can also occur in medium to low plasticity clays such as the BIONICS test embankment (Stirling et al., 2018; Yu et al., 2021). The BIONICS test embankment is located 15 km to the east of this levee, and both are constructed of low to medium plasticity glacial till (Hughes et al., 2009). Given the similar soil type and environmental conditions, it is reasonable to assume that cracks may form in the levee, but no observations have to-date been made.

If desiccation cracks form in the top layer of the levee, this may lead to elevated hydraulic conductivities within the cracked layer, providing a flow pathway below the surface of the levee, reducing the level of protection below the designed height (Dyer et al., 2009). Stirling et al., (2021) and Yu et al. (2021) demonstrate that crack closure can take significantly longer to occur than the return of VMC to field saturated conditions. At Warden, the first elevated river levels occur (1 October 2022) before the embankment has fully wetted up (Figure 10A). Near-surface seepage is, therefore, a greater risk in early autumn, with the embankment likely having a lower factor of safety (Young and Hassan, 2005). For slope stability, desiccation cracking with the onset of autumn rain is known to cause a minimum in the factor of safety (Jamalinia et al., 2020). For levees, if cracks are present in autumn, they will allow the infiltration of flood water into the levee while its slope stability is at a minimum, maximising the risk of shallow slope failures due to flood drawdown (e.g. Kim et al., 2023; Polemio & Lollino, 2011).

6 Implications of climate change on levee performance

Since the levee's construction in 2007, it has performed as designed, including in December 2015, when the levee safely withstood a flood close to its designed height, which overtopped the neighbouring flood wall (Environment Agency, 2016). For the embankment to be at risk of future failure, it either has to experience a larger or longer flood or its performance must deteriorate. Climate change is expected to bring the UK hotter, drier summers and warmer, wetter winters, which will impact the long-term performance of the levee (Lowe et al., 2018); this will likely change flood recurrence intervals, the length and depth of drought conditions and the magnitude of the seasonal wetting and drying cycles that drive long term deterioration.

To assess how climate change may impact the long-term deterioration of levees and the risk of desiccation cracking, a relationship between drying depth and weather conditions must be established. Comparing the resistivity-derived drying front depth to the observed local weather conditions by calculating a SMD for the four annual drying cycles (

Figure 10B) shows that SMD generally correlates very well with drying depth. As the drying front develops during spring and summer there is a particularly strong correlation with a Pearsons correlation coefficient of -0.951 (

Figure 10B & Figure 10C). However, there are some discrepancies, the most pronounced in the summer of 2023, where SMD remains around -30 mm while there is no observed drying front, and the measured VMC is near saturated conditions (Figure 6A and

Figure 10A). The discrepancy is likely caused by the simplistic nature of the SMD calculation, and that the evapotranspiration calculation is only using air temperature, and not a full suite of weather variables.

To extrapolate the drying front depth into the future, we use the local (2.2 km) UKCP18 convection permitting climate model outputs representing the RCP8.5 emission scenario (Murphy et al., 2018). This model was selected as it is the closest resolution to the 1 km HadUK dataset, provides the same data (daily rainfall, minimum and maximum temperature values), generally has better agreement with observations, and can better represent the heavy summer rainfall events that can have a large impact on SMD (Fung et al., 2018). This local projection contains 12 member models that sample different potential future outcomes (Fung et al., 2018). To apply the climate models at the site scale, they must be biased corrected (Fung, 2018). Each of the 12 UKCP18 model data sets was corrected to the local HadUK weather data for the period 1990 to 2020. The temperature data was corrected using a mean additive approach where, on average, 0.73 °C and 1.74 °C was added to the daily modelled minimum and maximum temperatures respectively. For precipitation, a multiplicative bias correction was applied, where the modelled precipitation was multiplied by 0.77. Using the bias corrected climate data, SMD was calculated for the 12 models and translated into an estimated drying front depth using the derived correlation. The maximum estimated drying depth for each year is then extracted (Figure 11). It should be noted that due to the water stress limitation within the SMD calculation, the maximum SMD is 160 mm, which corresponds to a maximum possible drying depth of 1.35 m. The 5-year rolling average shows that from 1980 to 2020, the estimated maximum drying front depth is fairly constant at ~0.6 m. This is in broad agreement with the estimated drying front from the observed temperature and rainfall data (Figure 11). After 2020, under an RCP8.5 climate scenario the average projected drying depth increases steadily to over 1.0 m by 2080. This represents a significant increase in average drying depth, particularly as the embankment freeboard is just 0.6 m, about the current drying depth.

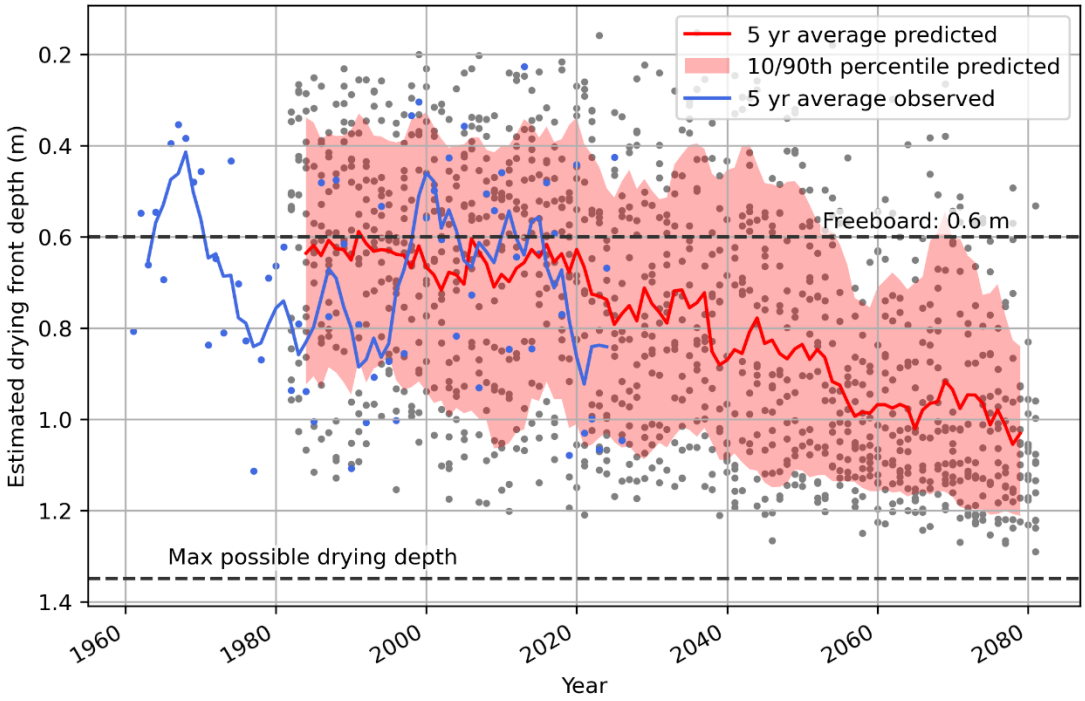

Figure 11. Projection of drying depth under the RCP 8.5 climate scenario using the local (2.2 km) UKCP18 climate projection. Grey dots = predicted max drying depth for each year for each model. Blue dots = estimated drying depth from HadUK observations. Freeboard at Warden is 0.6 m (Mott Macdonald, 2019). The maximum drying depth is the maximum depth when SMD reaches 160 mm. © University of Bristol & British Geological Survey © UKRI

While this correlation is based on a single study site, Warden is constructed of glacial till, a widely used and available material. Glacial till is less susceptible to drying than the high plasticity clays commonly found in the southeast. Therefore, these results are likely to be widely applicable, if not conservative, across the UK and in places where drought risk is increasing.

As the climate warms, the summer drying of levees will rapidly deepen average drying fronts over upcoming decades, increasing the environmental loading on the levee network. This will increase the chronic deterioration of levees as wetting and drying cycles regularly propagate deeper, degrading the soil structure and increasing permeability (Stirling et al., 2021). This may increase the risk of acute levee failure during autumnal flood events, where flood water exploits the still open crack networks below the surface, removing blocks enabling a breach to develop (Dyer et al., 2009).

7 Mitigation measures

While fissures have not been directly observed at Warden, there is potential for them to occur, encouraged by increasing summer SMD. To reduce the risk of the predicted increase in drying depths, measures may need to be taken to either mitigate the effect of fissuring or prevent fissuring from occurring in the first place (Table 3).

There are two key approaches to mitigating the effect of fissuring (Frith et al., 1997) (Table 3): 1) Increase the freeboard of the levee so the fissuring occurs in material above the designed level of protection. 2) Install a ~1.5 m deep cutoff wall (e.g. sheet piles) along the levee's crest to prevent seepage through the levee. Increasing the freeboard to match average projected drying depths by

2080 would require a ~0.5 m height extension to the designed level of protection based on the predicted increase in mean drying depth. While this would be effective, this would require a 50% increase in embankment volume for an embankment with Warden's current geometry. The added mass could also cause settlement issues. In contrast, adding a steel sheet pile cutoff wall would prevent seepage without the needed height increase. However, both solutions are expensive and have a high embedded carbon cost, making both potentially unattractive options.

Alternatively, preventative measures to minimise fissuring during dry conditions could be considered, for which there is a much larger range of options. These fall into three broad categories (Table 3): 1) Use materials that do not crack or mechanically prevent cracking (Frith et al., 1997), 2) Implement measures that reduce water loss from the levee, and 3) Irrigate the levee during dry conditions (Van Lanen et al., 2016).

	Method		Pros	Cons
Mitigation	Increase levee freeboard		Likely can use locally available materials	Requires a lot of material; increases land take; enhance settlement issues; requires excavation of levee
	Cut off wall		Prevents seepage; relatively quick to install	High CO2 cost of steel
Prevention	Crack resistance	Place self binding material (e.g. Hoggin)	Crack resistant; can be used below design height.	Import specialist material; relatively expensive; requires excavation of levee
		Mix sand and gravel into clay levee	Less material required than using Hoggin; improves overtopping resistance	Likely import of materials; requires excavation and mixing levee soil
		Place Geogrid	Binds soil together; Reduces the macro cracks; may stop animal burrowing	Does not prevent fine cracking, requires excavation of levee surface
	Water loss	Impermeable geotextile	Prevent desiccation below membrane – reduce fissures;	Faster wilting and dying of vegetation; increased risk of overtopping erosion; shallow slope failure along membrane
		Soil vapour barrier	Reduce desiccation below membrane.	Likely import of materials
		Reseed with low water-use grass mix	Reduce evapotranspiration; relatively non invasive	Limited choice of native plants; impact on overtopping; biodiversity loss; root structure
		Shade levee	Reduced evapotranspiration by up to 30%; dual land use if photovoltaics used.	Likely expensive; large visual impact; scour risk around supports; impede grass mowing
	Irrigation of levee		Directly reduces the SMD	Effectiveness is uncertain; require water during droughts; has to be done regularly

Table 3. Mitigation and prevention methods for reducing the effect of drying conditions on levees and the formation of desiccation cracks (CIRIA et al., 2013, sec. 9.12.2; Frith et al., 1997). Financial considerations excluded.

Placing materials that do not crack within the desiccated top layer of a levee will mitigate the effect of hotter, drier summers. This could include using self-binding gravel (Hoggin), which can be included within the level of protection, so it does not need to raise the level of the embankment. Alternatively, sand and gravel may be mixed into a clay rich levee material to

prevent shrink swell. This also improves the levee's ability to withstand overtopping erosion (Sekine et al., 2020). Finally, a geogrid may be installed to bind the soil together and prevent macro cracking, but fine fissuring can still occur (Frith et al., 1997).

A different approach can focus on reducing water loss from the embankment during dry periods. This can be a physical barrier to prevent evaporation from the soil, such as plastic sheeting buried below the topsoil (Frith et al., 1997) or an engineered soil water barrier (Tsiampousi et al., 2024). Alternatively, low water-use grass mixes could be chosen to minimise evapotranspiration (Garwood and Sinclair, 1979). Those with C4 photosynthesis pathways use much less water than C3 (Johnston et al., 2002). However, few native plants in Northern Europe use the C4 pathway; importing species or using genetically modified plants will raise ethical and conservation issues. Finally, shading of the levee, such as by a solar panel canopy, can reduce water loss by as much as 30% due to reduced solar radiation (Marrou et al., 2013). Overall, retrofitting levees to cope with increasing drying depths is highly invasive, and almost all methods require at least the stripping of the topsoil or cracked layer.

Finally, if an immediate response is necessary to reduce desiccation cracking within a levee, it may be irrigated. This is commonly implemented in the Netherlands on old peat levees based on visual inspection (Van Lanen et al., 2016). However, this is a short-term solution, and it is unlikely to be sustainable or cost-effective in the long term. In drought conditions, it may not be an acceptable use of water.

8 Conclusion

The effect of environmental loading on the levee at Warden has been assessed through the integration of subsurface resistivity monitoring and environmental sensors over 4 years. The resistivity monitoring reveals clear subsurface changes in moisture content in response to the environmental loading on the levee. This identified two possible deterioration pathways that could result in levee failure in the future: 1) seepage through the granular foundation strata could facilitate backwards erosion that develops into a piping failure during a flood event; 2) desiccation of the embankment crest could create a connected crack network that flood water might exploit and initiate concentrated leak erosion that develops into a full breach.

Climate change will bring hotter, drier summers, increasing the drying depth from 0.6 m to over 1 m towards the end of the 21st century. This will accelerate the decadal deterioration of the soil structure and, in turn, may increase the hydraulic conductivity of the levee. In hot, dry summers of the future, levees will become increasingly vulnerable to deep cracks and associated seepage through the crest during the first floods of autumn. A growing focus will be needed to build and repair existing levees to minimise the effect of larger soil moisture deficits and the associated cracking risk.

Acknowledgements

We would like to acknowledge Arnaud Watlet for installing the monitoring equipment and the Environment Agency for providing access to the site, and the two anonymous reviewers for constructive feedback. This work was funded by a NERC GW4+ UK Doctoral Training

Partnership Studentship (Grant NE/L002434/1), the BGS University Funding Initiative (S337), and the ACHILLES project (EP/R034575/1). Adrian White, Paul Wilkinson, Jonathan Chambers, and James Boyd publish with the permission of the Executive Director, British Geological Survey (UKRI-NERC).

Data Availability

The data are available from Adrian White (adwh@bgs.ac.uk) upon request.

References

Allen, R.G., Pereira, L.S., Raes, D., Smith, M., 1998. Crop evapotranspiration: guidelines for computing crop water requirements. In: FAO Irrigation and Drainage Paper No. 56. Rome, Italy.

Amabile, A., de Carvalho Faria Lima Lopes, B., Pozzato, A., Benes, V., Tarantino, A., 2020. An assessment of ERT as a method to monitor water content regime in flood embankments: The case study of the Adige River embankment. Physics and Chemistry of the Earth, 120, 1–10. https://doi.org/10.1016/j.pce.2020.102930

Archer, D.R., Leesch, F., Harwood, K., 2007a. Learning from the extreme River Tyne flood in January 2005. Water and Environment Journal 21, 133–141. https://doi.org/10.1111/j.1747-6593.2006.00058.x

Archer, D.R., Leesch, F., Harwood, K., 2007b. Assessment of severity of the extreme River Tyne flood in January 2005 using gauged and historical information. Hydrological Sciences Journal 52, 992–1003. https://doi.org/10.1623/hysj.52.5.992

Bayoumi, A., Meguid, M.A., 2011. Wildlife and safety of earthen structures: A review. Journal of Failure Analysis and Prevention 11, 295–319. https://doi.org/10.1007/s11668-011-9439-y

Bettess, R., Reeve, C.E., 1995. Performance of River Flood Embankments. Report SR 384. Wallingford.

Bièvre, G., Oxarango, L., Günther, T., Goutaland, D., Massardi, M., 2018. Improvement of 2D ERT measurements conducted along a small earth-filled dyke using 3D topographic data and 3D computation of geometric factors. J Appl Geophy 153, 100–112. https://doi.org/10.1016/j.jappgeo.2018.04.012

Binley, A., Slater, L., 2020. Resistivity and Induced Polarization. Cambridge University Press. https://doi.org/10.1017/9781108685955

Blake, A., Smethurst, J., Yu, Z., Brooks, H., Stirling, R., Holmes, J., Watlet, A., Whiteley, J., Chambers, J., Hughes, P., Smith, A., Briggs, K., 2022. Long-term monitoring of long linear geotechnical infrastructure for a deeper understanding of deterioration processes, in: 11th International Symposium on Field Monitoring in Geomechanics. pp. 1–7.

626 Blanchy, G., Saneiyan, S., Boyd, J., McLachlan, P., Binley, A., 2020. ResIPy, an intuitive open
627 source software for complex geoelectrical inversion/modeling. Comput Geosci 137.
628 https://doi.org/10.1016/j.cageo.2020.104423

629 Boyd, J., Chambers, J., Wilkinson, P., Peppa, M., Watlet, A., Kirkham, M., Jones, L., Swift, R.,
630 Meldrum, P., Uhlemann, S., Binley, A., 2021. A linked geomorphological and geophysical
631 modelling methodology applied to an active landslide. Landslides 18, 2689–2704.
632 https://doi.org/10.1007/s10346-021-01666-w

633 Boyd, J.P., Binley, A., Wilkinson, P., Holmes, J., Bruce, E., Chambers, J., 2024. Practical
634 considerations for using petrophysics and geoelectrical methods on clay rich landslides. Eng
635 Geol 334, 1–14. https://doi.org/10.1016/j.enggeo.2024.107506

636 British Geological Survey, 1975. Hexham, Enagland and Wales Sheet 19, Bedrock geology,
637 1:50000 Geological Map Series.

638 Brunet, P., Clément, R., Bouvier, C., 2010. Monitoring soil water content and deficit using
639 Electrical Resistivity Tomography (ERT) - A case study in the Cevennes area, France. J
640 Hydrol (Amst) 380, 146–153. https://doi.org/10.1016/j.jhydrol.2009.10.032

641 Burns, D., Miller, H., 1883. Hexham, Allendale, Haltwhistle. England and Wales Sheet 19,
642 1:63,360 geological map series.

643 Chambers, J.E., Gunn, D.A., Wilkinson, P.B., Meldrum, P.I., Haslam, E., Holyoake, S., Kirkham,
644 M., Kuras, O., Merritt, A., Wragg, J., 2014. 4D electrical resistivity tomography monitoring
645 of soil moisture dynamics in an operational railway embankment. Near Surface Geophysics
646 12, 61–72. https://doi.org/10.3997/1873-0604.2013002

647 CIRIA, Ministry of Ecology, USACE, 2013. The International Levee Handbook. CIRIA.

648 Clarke, D., Smethurst, J.A., 2010. Effects of climate change on cycles of wetting and drying in
649 engineered clay slopes in England. Quarterly Journal of Engineering Geology and
650 Hydrogeology 43, 473–486. https://doi.org/10.1144/1470-9236/08-106

651 Dahlin, T., Zhou, B., 2004. A numerical comparison of 2D resistivity imaging with 10 electrode
652 arrays. Geophys Prospect 52, 379–398. https://doi.org/10.1111/j.1365-2478.2004.00423.x

653 Dixon, N., Crosby, C.J., Stirling, R., Hughes, P.N., Smethurst, J., Briggs, K., Hughes, D., Gunn, D.,
654 Hobbs, P., Loveridge, F., Glendinning, S., Dijkstra, T., Hudson, A., 2019. *In situ*
655 measurements of near-surface hydraulic conductivity in engineered clay slopes. Quarterly
656 Journal of Engineering Geology and Hydrogeology 52, 123–135.
657 https://doi.org/10.1144/qjegh2017-059

658 Dyer, M., 2004. Performance of flood embankments in England and Wales. Proceedings of the
659 Institution of Civil Engineers: Water Management 157, 177–186.
660 https://doi.org/10.1680/wama.2004.157.4.177

661 Dyer, M., Utili, S., Zielinski, M., 2009. Field survey of desiccation fissuring of flood
662 embankments. Proceedings of the Institution of Civil Engineers: Water Management 162,
663 221–232. https://doi.org/10.1680/wama.2009.162.3.221

664 Environment Agency, 2020. AIMS Spatial Flood Defences (inc. standardised attributes) [WWW
665 Document]. DEFRA Data Services. URL

https://environment.data.gov.uk/dataset/8e5be50f-d465-11e4-ba9a-f0def148f590 (accessed 1.18.24).

Environment Agency, 2016. Impact Report Winter Flooding 2015-16.

Evening Chronicle, 2007. FLOOD defences are being rebuilt as part of a Tyneside facelift. Evening Chronicle (Newcastle, England).

Frith, C.W., Purcell, A.M., Powell, A.S., 1997. Earth embankment fissuring manual, Technical report W41.

Fung, F., 2018. How to Bias Correct, UKCP18 Guidance. Exeter.

Fung, F., Lowe, J., Mitchell, J., Murphy, J., Bernie, D., Gohar, L., Harris, G., Howard, T., Kendon, E., Maisey, P., Palmer, M., Sexton, D., 2018. UKCP18 Guidance: How to use the UKCP18 Land Projections. Exeter.

Garwood, E.A., Sinclair, J., 1979. Use of water by six grass species. 2. Root distribution and use of soil water. J Agric Sci 93, 25–35. https://doi.org/10.1017/S0021859600086081

Gunn, D.A., Chambers, J.E., Uhlemann, S., Wilkinson, P.B., Meldrum, P.I., Dijkstra, T.A., Haslam, E., Kirkham, M., Wragg, J., Holyoake, S., Hughes, P.N., Hen-Jones, R., Glendinning, S., 2015. Moisture monitoring in clay embankments using electrical resistivity tomography. Constr Build Mater 92, 82–94. https://doi.org/10.1016/j.conbuildmat.2014.06.007

Helm, P., Stirling, R., Glendinning, S., 2016. The Implications of Using Estimated Solar Radiation on the Derivation of Potential Evapotranspiration and Soil Moisture Deficit within an Embankment. Procedia Eng 143, 697–707. https://doi.org/10.1016/j.proeng.2016.06.105

Hojat, A., Arosio, D., Ivanov, V.I., Loke, M.H., Longoni, L., Papini, M., Tresoldi, G., Zanzi, L., 2020. Quantifying seasonal 3D effects for a permanent electrical resistivity tomography monitoring system along the embankment of an irrigation canal. Near Surface Geophysics 18, 427–443. https://doi.org/10.1002/nsg.12110

Holmes, J., Chambers, J., Wilkinson, P., Dashwood, B., Gunn, D., Cimpoiașu, M., Kirkham, M., Uhlemann, S., Meldrum, P., Kuras, O., Huntley, D., Abbott, S., Sivakumar, V., Donohue, S., 2022. 4D electrical resistivity tomography for assessing the influence of vegetation and subsurface moisture on railway cutting condition. Eng Geol 307, 1–13. https://doi.org/10.1016/j.enggeo.2022.106790

Hughes, P.N., Glendinning, S., Mendes, J., Parkin, G., Toll, D.G., Gallipoli, D., Miller, P.E., 2009. Full-scale testing to assess climate effects on embankments. Proceedings of the Institution of Civil Engineers: Bridge Engineering 162, 67–79. https://doi.org/10.1680/ensu.2009.162.2.67

Hui, R., Jachens, E., Lund, J., 2016. Risk-based planning analysis for a single levee. Water Resour Res 52, 2513–2528. https://doi.org/10.1002/2014WR016478

IPCC, 2023. Climate Change 2023: Synthesis Report. Contribution of Working Groups I, II and III to the Sixth Assessment Report of the Intergovernmental Panel on Climate Change [Core Writing Team, H. Lee and J. Romero (eds.)], Proceedings of the Institution of Civil Engineers - Water Management. Geneva, Switzerland.

Islam, M.R., Fereshtehpour, M., Najafi, M.R., Khaliq, M.N., Khan, A.A., Sushama, L., Nguyen, V.T.V., Elshorbagy, A., Roy, R., Wilson, A., Perdikaris, J., Masud, M.B., Khan, M.S., 2024. Climate-resilience of dams and levees in Canada: a review. Discover Applied Sciences. https://doi.org/10.1007/s42452-024-05814-4

Jamalinia, E., Vardon, P.J., Steele-Dunne, S.C., 2020. The impact of evaporation induced cracks and precipitation on temporal slope stability. Comput Geotech 122, 1–10. https://doi.org/10.1016/j.compgeo.2020.103506

Janga, J.K., Reddy, K.R., Schulenberg, J., 2024. Climate change impacts on safety of levees: A Review, in: Geotechnical Engineering Challenges to Meet Current and Emerging Needs of Society. CRC Press, pp. 1669–1674. https://doi.org/10.1201/9781003431749-310

Jodry, C., Palma Lopes, S., Fargier, Y., Sanchez, M., Côte, P., 2019. 2D-ERT monitoring of soil moisture seasonal behaviour in a river levee: A case study. J Appl Geophy 167, 140–151. https://doi.org/10.1016/j.jappgeo.2019.05.008

Johnston, I., Murphy, W., Holden, J., 2021. A review of floodwater impacts on the stability of transportation embankments. Earth Sci Rev 215, 1–15. https://doi.org/10.1016/j.earscirev.2021.103553

Johnston, W.H., Koen, T.B., Shoemark, V.F., 2002. Water use, competition and a temperate-zone C4 grass (Eragrostis curvula (Schrad.) Nees. complex) cv. Consol. Aust J Agric Res 53, 715. https://doi.org/10.1071/AR98115

Jones, G., Sentenac, P., Zielinski, M., 2014. Desiccation cracking detection using 2-D and 3-D electrical resistivity tomography: Validation on a flood embankment. J Appl Geophy 106, 196–211. https://doi.org/10.1016/j.jappgeo.2014.04.018

LaBrecque, D.J., Yang, X., 2000. Difference Inversion of ERT Data: A Fast Inversion Method for 3-D In-Situ Monitoring, in: Symposium on the Application of Geophysics to Engineering and Environmental Problems 2000. Environment and Engineering Geophysical Society, pp. 907–914. https://doi.org/10.4133/1.2922831

Loke, M.H., Chambers, J.E., Rucker, D.F., Kuras, O., Wilkinson, P.B., 2013. Recent developments in the direct-current geoelectrical imaging method. J Appl Geophy 95, 135–156. https://doi.org/10.1016/j.jappgeo.2013.02.017

Lowe, J.A., Bernie, D., Bett, P., Bricheno, L., Brown, S., Calvert, D., Clark, R., Eagle, K., Edwards, T., Fosser, G., 2018. UKCP18 science overview report, Met Office Hadley Centre: Exeter, UK. Exeter.

Ma, R., McBratney, A., Whelan, B., Minasny, B., Short, M., 2011. Comparing temperature correction models for soil electrical conductivity measurement. Precis Agric 12, 55–66. https://doi.org/10.1007/s11119-009-9156-7

Marrou, H., Dufour, L., Wery, J., 2013. How does a shelter of solar panels influence water flows in a soil–crop system? European Journal of Agronomy 50, 38–51. https://doi.org/10.1016/j.eja.2013.05.004

743 Met Office, Hollis, D., McCarthy, M., Kendon, M., Legg, T., Simpson, I., 2018. HadUK-Grid
744 gridded and regional average climate observations for the UK. Centre for Environmental
745 Data Analysis.

746 Morris, M., Dyer, M., Smith, P., 2007. Management of Flood Embankments: A good practice
747 review. R&D Technical Report FD2411/TR1. London.

748 Mott Macdonald, 2019. North East Structural Assessments: Warden Flood Defences - Visual
749 inspection. Newcastle.

750 Murphy, J.M., Harris, G.R., Sexton, E.J., Kendon, P.E., Bett, P.E., Clark, K.E., Eagle, K.E., Fosser,
751 G., Fung, F., Lowe, J.A., McDonald, R.E., McInnes, R.N., McSweeney, C.F., Mitchell, J.F.B.,
752 Rostron, J.W., Thornton, H.E., Tucker, S., Yamazaki, K., 2018. UKCP18 Land Projections:
753 Science Report.

754 Northumberland County Council, 2016. Northumberland County Council Flood Action Plan.
755 Cramlington, Northumberland.

756 Orlandini, S., Moretti, G., Albertson, J.D., 2015. Evidence of an emerging levee failure mechanism
757 causing disastrous floods in Italy. Water Resour Res 51, 7995–8011.
758 https://doi.org/10.1002/2015WR017426

759 Özer, I.E., van Damme, M., Jonkman, S.N., 2019. Towards an International Levee Performance
760 Database (ILPD) and Its Use for Macro-Scale Analysis of Levee Breaches and Failures. Water
761 (Basel) 12, 1–22. https://doi.org/10.3390/w12010119

762 Passmore, D.G., Macklin, M.G., 2000. Late Holocene channel and floodplain development in a
763 wandering gravel-bed river: The River South Tyne at Lambley, Northern England. Earth Surf
764 Process Landf 25, 1237–1256. https://doi.org/10.1002/1096-9837(200010)25:11<1237::AID-
765 ESP134>3.0.CO;2-S

766 Pistrika, A.K., Jonkman, S.N., 2010. Damage to residential buildings due to flooding of New
767 Orleans after hurricane Katrina. Natural Hazards 54, 413–434.
768 https://doi.org/10.1007/s11069-009-9476-y

769 Polemio, M., Lollino, P., 2011. Failure of infrastructure embankments induced by flooding and
770 seepage: A neglected source of hazard. Natural Hazards and Earth System Science 11, 3383–
771 3396. https://doi.org/10.5194/nhess-11-3383-2011

772 Raković, M., Pujević, V., Jocković, S., Obradović, N., 2024. Adaptability of flood embankments
773 to climate change.

774 River Levels, 2024. River South Tyne at Warden Bridge End [WWW Document]. URL
775 https://riverlevels.uk/northumberland-warden-warden-bridge-end (accessed 1.16.24).

776 Robertson, P.K., 1990. Soil classification using the cone penetration test. Canadian Geotechnical
777 Journal 27, 151–158. https://doi.org/10.1139/t90-014

778 Robinson, J.D., Vahedifard, F., 2016. Weakening mechanisms imposed on California's levees
779 under multiyear extreme drought. Clim Change 137, 1–14. https://doi.org/10.1007/s10584-
780 016-1649-6

781 Rouainia, M., Helm, P., Davies, O., Glendinning, S., 2020. Deterioration of an infrastructure
782 cutting subjected to climate change. Acta Geotech 15, 2997–3016.
783 https://doi.org/10.1007/s11440-020-00965-1

784 Samaniego, L., Thober, S., Kumar, R., Wanders, N., Rakovec, O., Pan, M., Zink, M., Sheffield, J.,
785 Wood, E.F., Marx, A., 2018. Anthropogenic warming exacerbates European soil moisture
786 droughts. Nat Clim Chang 8, 421–426. https://doi.org/10.1038/s41558-018-0138-5

787 Sekine, M., Matsuura, T., Hirokawa, M.O.E., Suga, T., 2020. Influence of sediment compostition
788 on breaching process of model river levee, in: 22nd IAHR-APD Congress. pp. 1–4.

789 Semmens, S., Zhou, W., 2021. Predicting backward erosion piping hazard, Lower Mississippi
790 Valley, USA. Quarterly Journal of Engineering Geology and Hydrogeology 54, 1–7.
791 https://doi.org/10.1144/qjegh2020-035

792 Sentenac, P., Jones, G., Zielinski, M., Tarantino, A., 2012. An approach for the geophysical
793 assessment of fissuring of estuary and river flood embankments: Validation against two case
794 studies in England and Scotland. Environ Earth Sci 69, 1939–1949.
795 https://doi.org/10.1007/s12665-012-2026-z

796 Simm, J., Flikweert, J.-J., Hollingsworth, C., Tarrant, O., 2017. Ten years of lessons learned from
797 English levee performance during severe flood events, in: 5th Annual Meeting of
798 International Commission on Large Dams. Prague, Czech Republic: ICOLD. p. 9.

799 Simm, J., Wallis, M., Smith, P., Tourment, R., Veylon, G., Deniaud, Y., Durand, E., McVicker, J.,
800 Hersh-Burdick, R., 2012. The significance of failure modes in the design and management
801 of levees—a perspective from the International Levee Handbook team. Comprehensive
802 Flood Risk Management 1–15. https://doi.org/10.1201/b13715-43

803 Smethurst, J.A., Clarke, D., Powrie, W., 2006. Seasonal changes in pore water pressure in a grass-
804 covered cut slope in London Clay. Géotechnique 56, 523–537.
805 https://doi.org/10.1680/geot.2006.56.8.523

806 Smith, K., Hinchsliffe, K., Harding, Mike, 2009. Flood embankment vegetation management
807 trials : final report. Science project SC030228/SR1. Environment Agency, Bristol.

808 Stirling, R.A., Glendinning, S., Davie, C.T., Hughes, P.N., 2018. The Behaviour and Influence of
809 Desiccation Cracking on a Full-Scale , Vegetated Infrastructure Embankment. Proceedings
810 of the 7th International Conference on Unsaturated Soils 2–7.

811 Stirling, R.A., Toll, D.G., Glendinning, S., Helm, P.R., Yildiz, A., Hughes, P.N., Asquith, J.D., 2021.
812 Weather-driven deterioration processes affecting the performance of embankment slopes.
813 Géotechnique 71, 957–969. https://doi.org/10.1680/jgeot.19.SiP.038

814 Tarrant, O., Hambidge, C., Hollingsworth, C., Normandale, D., Burdett, S., 2017. Identifying the
815 signs of weakness, deterioration, and damage to flood defence infrastructure from remotely
816 sensed data and mapped information. J Flood Risk Manag 11, 317–330.
817 https://doi.org/10.1111/jfr3.12326

818 Thaimo, F., Ekolu, S.O., Quainoo, H., 2021. Standard relationship between plasticity index and
819 linear shrinkage: revisited. Proceedings of the Institution of Civil Engineers: Geotechnical
820 Engineering 176, 211–219. https://doi.org/10.1680/jgeen.21.00085

Tresoldi, G., Arosio, D., Hojat, A., Longoni, L., Papini, M., Zanzi, L., 2019. Long-term hydrogeophysical monitoring of the internal conditions of river levees. Eng Geol 259, 1–11. https://doi.org/10.1016/j.enggeo.2019.05.016

Tsiampousi, A., Day, C., Petalas, A., 2024. Engineering soil barriers to minimise annual shrinkage/swelling in plastic clays. Geomechanics for Energy and the Environment 38, 1–17. https://doi.org/10.1016/j.gete.2024.100540

Tso, C.H.M., Kuras, O., Binley, A., 2019. On the Field Estimation of Moisture Content Using Electrical Geophysics: The Impact of Petrophysical Model Uncertainty. Water Resour Res 55, 7196–7211. https://doi.org/10.1029/2019WR024964

Tso, C.H.M., Kuras, O., Wilkinson, P.B., Uhlemann, S., Chambers, J.E., Meldrum, P.I., Graham, J., Sherlock, E.F., Binley, A., 2017. Improved characterisation and modelling of measurement errors in electrical resistivity tomography (ERT) surveys. J Appl Geophy 146, 103–119. https://doi.org/10.1016/j.jappgeo.2017.09.009

Uhlemann, S., Chambers, J., Wilkinson, P., Maurer, H., Merritt, A., Meldrum, P., Kuras, O., Gunn, D., Smith, A., Dijkstra, T., 2017. Four-dimensional imaging of moisture dynamics during landslide reactivation. J Geophys Res Earth Surf 122, 398–418. https://doi.org/10.1002/2016JF003983

Van Lanen, H.A.J., Laaha, G., Kingston, D.G., Gauster, T., Ionita, M., Vidal, J., Vlnas, R., Tallaksen, L.M., Stahl, K., Hannaford, J., Delus, C., Fendekova, M., Mediero, L., Prudhomme, C., Rets, E., Romanowicz, R.J., Gailliez, S., Wong, W.K., Adler, M., Blauhut, V., Caillouet, L., Chelcea, S., Frolova, N., Gudmundsson, L., Hanel, M., Haslinger, K., Kireeva, M., Osuch, M., Sauquet, E., Stagge, J.H., Van Loon, A.F., 2016. Hydrology needed to manage droughts: the 2015 European case. Hydrol Process 30, 3097–3104. https://doi.org/10.1002/hyp.10838

Vannoppen, W., Poesen, J., Peeters, P., De Baets, S., Vandevoorde, B., 2016. Root properties of vegetation communities and their impact on the erosion resistance of river dikes. Earth Surf Process Landf 41, 2038–2046. https://doi.org/10.1002/esp.3970

Waxman, M.H., Smits, L.J.M., 1968. Electrical Conductivities in Oil-Bearing Shaly Sands. Society of Petroleum Engineers Journal 8, 107–122. https://doi.org/10.2118/1863-A

White, A., Boyd, J., Wilkinson, P., Unwin, H.E., Wookey, J., Kendall, J.M., Binley, A., Chambers, J., 2024. Assessing the effect of offline topography on electrical resistivity measurements: insights from flood embankments. Geophys J Int. https://doi.org/10.1093/gji/ggae313

White, A., Watlet, A., Blake, A., Wilkinson, P., Dashwood, B., Chambers, J., 2023. Multi-Scale Characterisation of a Clay Flood Embankment, Warden, Northumberland, in: NSG2023 29th European Meeting of Environmental and Engineering Geophysics. European Association of Geoscientists & Engineers, pp. 1–5. https://doi.org/10.3997/2214-4609.202320210

Young, M.J., Hassan, R.M., 2005. Grass cover layer failure on the inner slope of dikes. Institute for Water Education, Delft, Netherlands. https://doi.org/10.1142/9789812709554_0241

Yu, Z., Eminue, O.O., Stirling, R., Davie, C., Glendinning, S., 2021. Desiccation cracking at field scale on a vegetated infrastructure embankment. Geotechnique Letters 11, 88–95. https://doi.org/10.1680/jgele.20.00108

Zhang, L., Peng, M., Chang, D.D., Xu, Y., 2016. Dam Failure Mechanisms and Risk Assessment, 1st ed, Dam Failure Mechanisms and Risk Assessment. John Wiley & Sons, Singapore. https://doi.org/10.1002/9781118558522